Integrated mutational landscape analysis of uterine leiomyosarcomas

Jungmin Choi[a,b,1], Aranzazu Manzano[c,1], Weilai Dong[b,d,1], Stefania Bellone[c], Elena Bonazzoli[c], Luca Zammataro[c], Xiaotong Yao[e,f,g], Aditya Deshpande[e,f,g], Samir Zaidi[h], Adele Guglielmi[c], Barbara Gnutti[c], Nupur Nagarkatti[c], Joan R. Tymon-Rosario[c], Justin Harold[c], Dennis Mauricio[c], Burak Zeybek[c], Gulden Menderes[c], Gary Altwerger[c], Kyungjo Jeong[a], Siming Zhao[i], Natalia Buza[j], Pei Hui[j], Antonella Ravaggi[k], Eliana Bignotti[k], Chiara Romani[k], Paola Todeschini[k], Laura Zanotti[k], Franco Odicino[k], Sergio Pecorelli[k], Laura Ardighieri[l], Kaya Bilguvar[b], Charles M. Quick[m], Dan-Arin Silasi[n], Gloria S. Huang[c], Vaagn Andikyan[c], Mitchell Clark[c], Elena Ratner[c], Masoud Azodi[c], Marcin Imielinski[e,f], Peter E. Schwartz[c], Ludmil B. Alexandrov[o], Richard P. Lifton[d], Joseph Schlessinger[p,2], and Alessandro D. Santin[c]

[a]Department of Biomedical Sciences, Korea University College of Medicine, 02841 Seoul, Korea; [b]Department of Genetics, Yale University School of Medicine, New Haven, CT 06510; [c]Department of Obstetrics, Gynecology and Reproductive Sciences, Yale University School of Medicine, New Haven, CT 06510; [d]Laboratory of Human Genetics and Genomics, The Rockefeller University, New York, NY 10065; [e]Department of Pathology and Laboratory Medicine, Weill Cornell Medicine, New York, NY; [f]New York Genome Center, New York, NY 10013; [g]Triinstitutional PhD Program in Computational Biology and Medicine, Weill Cornell Medicine, New York, NY 10021; [h]Human Oncology and Pathogenesis Program, Memorial Sloan Kettering Cancer Center, New York, NY 10065; [i]Department of Human Genetics, University of Chicago, Chicago, IL 60637; [j]Department of Pathology, Yale University School of Medicine, New Haven, CT 06510; [k]Department of Obstetrics and Gynecology, "Angelo Nocivelli" Institute of Molecular Medicine, University of Brescia, 25100 Brescia, Italy; [l]Department of Pathology, University of Brescia, Azienda Socio Sanitaria Territoriale degli Spedali Civili di Brescia, 25100 Brescia, Italy; [m]Department of Pathology, University of Arkansas for Medical sciences, Little Rock, AR 72205; [n]Division of Gynecologic Oncology, Mercy Clinic, St. Louis, MO 63141; [o]Department of Cellular and Molecular Medicine, University of California San Diego, La Jolla, CA 92093; and [p]Department of Pharmacology, Yale University School of Medicine, New Haven, CT 06510

Contributed by Joseph Schlessinger, February 16, 2021 (sent for review November 30, 2020; reviewed by Gottfried E. Konecny and John A. Martignetti)

Uterine leiomyosarcomas (uLMS) are aggressive tumors arising from the smooth muscle layer of the uterus. We analyzed 83 uLMS sample genetics, including 56 from Yale and 27 from The Cancer Genome Atlas (TCGA). Among them, a total of 55 Yale samples including two patient-derived xenografts (PDXs) and 27 TCGA samples have whole-exome sequencing (WES) data; 10 Yale and 27 TCGA samples have RNA-sequencing (RNA-Seq) data; and 11 Yale and 10 TCGA samples have whole-genome sequencing (WGS) data. We found recurrent somatic mutations in TP53, MED12, and PTEN genes. Top somatic mutated genes included TP53, ATRX, PTEN, and MEN1 genes. Somatic copy number variation (CNV) analysis identified 8 copy-number gains, including 5p15.33 (TERT), 8q24.21 (C-MYC), and 17p11.2 (MYOCD, MAP2K4) amplifications and 29 copy-number losses. Fusions involving tumor suppressors or oncogenes were deetected, with most fusions disrupting RB1, TP53, and ATRX/DAXX, and one fusion (ACTG2-ALK) being potentially targetable. WGS results demonstrated that 76% (16 of 21) of the samples harbored chromoplexy and/or chromothripsis. Clinically actionable mutational signatures of homologous-recombination DNA-repair deficiency (HRD) and microsatellite instability (MSI) were identified in 25% (12 of 48) and 2% (1 of 48) of fresh frozen uLMS, respectively. Finally, we found olaparib (PARPi; $P = 0.002$), GS-626510 (C-MYC/BETi; $P < 0.000001$ and $P = 0.0005$), and copanlisib (PIK3CAi; $P = 0.0001$) monotherapy to significantly inhibit uLMS-PDXs harboring derangements in C-MYC and PTEN/PIK3CA/AKT genes (LEY11) and/or HRD signatures (LEY16) compared to vehicle-treated mice. These findings define the genetic landscape of uLMS and suggest that a subset of uLMS may benefit from existing PARP-, PIK3CA-, and C-MYC/BET-targeted drugs.

uterine leiomyosarcomas | whole-exome sequencing | whole-genome sequencing | mutational landscape

Uterine leiomyosarcomas (uLMS) are highly lethal gynecologic sarcomas arising from the myometrium, the smooth muscle layer of the uterus. They represent the most common type of uterine sarcomas (i.e., 80% of all uterine sarcomas), which overall account for 3 to 7% of all uterine cancers (1). LMS have poor prognosis and are characterized by aggressive biological behavior, leading to early local and distant metastatic spread. While surgery represents the treatment of choice and can be curative in about 50% of early-stage disease (i.e., stage I), advanced or recurrent disease is minimally responsive to current standard adjuvant treatments, including chemotherapy, radiation, or immunotherapy (1). A deeper understanding of the molecular basis of uLMS and the development of novel, more effective treatment modalities remain an unmet medical need.

Significance

Identification of novel, effective treatment modalities for patients with uterine leiomyosarcomas (uLMS) remains an unmet medical need. Using an integrated whole-genome, whole-exome, and RNA-Seq analysis, we identified recurrently mutated genes and deranged pathways, including the homologous-recombination repair (HRR) pathway deficiency (HRD), alternative lengthening of telomere (ALT), C-MYC/BET, and PI3K-AKT-mTOR pathways as potential targets. Using two fully sequenced patient-derived xenografts (PDXs) harboring deranged C-MYC/BET and PTEN/PIK3CA pathways and/or an HRD signature (i.e., LEY11 and LEY16), we found olaparib (PARPi), GS-626510 (BETi), and copanlisib (PIK3CAi) monotherapy to significantly inhibit in vivo uLMS PDXs growth. Our integrated genetic analysis, combined with in vivo preclinical validation experiments, suggests that a large subset of uLMS may potentially benefit from existing PARPi/BETi/PIK3CAi-targeted drugs.

Author contributions: R.P.L., J.S., and A.D.S. designed research; S.B., E. Bonazzoli, L. Zammataro, A.G., B.G., N.N., J.R.T.-R., J.H., D.M., B.Z., G.M., G.A., N.B., P.H., A.R., E. Bignotti, C.R., P.T., L. Zanotti, F.O., S.P., L.A., and V.A. performed research; K.B., C.M.Q., D.-A.S., G.S.H., E.R., M.A., M.I., P.E.S., and L.B.A. contributed new reagents/analytic tools; J.C., A.M., W.D., X.Y., A.D., S. Zaidi, K.J., S. Zhao, R.P.L., J.S., and A.D.S. analyzed data; and J.C., A.M., W.D., S. Zaidi, S. Zhao, M.C., J.S., and A.D.S. wrote the paper.

Reviewers: G.E.K., David Geffen School of Medicine at UCLA; and J.A.M., Mount Sinai School of Medicine.

The authors declare no competing interest.

Published under the PNAS license.

[1]J.C., A.M., and W.D. contributed equally to this work.

[2]To whom correspondence may be addressed. Email: Joseph.Schlessinger@Yale.edu.

This article contains supporting information online at https://www.pnas.org/lookup/suppl/doi:10.1073/pnas.2025182118/-/DCSupplemental.

Published April 5, 2021.

Downloaded at Palestinian Territory, occupied on November 27, 2021

www.manaraa.com

A limited number of studies have comprehensively evaluated the genetic landscape of uLMS. The majority have analyzed a low number of uLMS combined with a much larger number of LMS arising from nongynecologic organs (2–5). Accordingly, in this study, we have used whole-genome sequencing (WGS), whole-exome sequencing (WES), and RNA sequencing (RNA-Seq) to perform an integrated analysis of a large cohort of fresh and formalin-fixed uLMS, including two patient-derived xenografts (PDXs). Our results reveal multiple genes harbor recurrent mutations and increased numbers of somatic single nucleotide variation (SNV) and copy number variation (CNV), as well as gene fusions and altered pathways including but not limited to the HRR pathway deficiency (HRD), alternative lengthening of telomere (ALT), chromatin remodeling, cell cycle, mitogen-activated protein kinase (MAPK), and PTEN/PI3KCA-AKT-m-TOR pathways. Importantly, the establishment of uLMS PDXs harboring derangements in the C-MYC/BET and PTEN/PIK3CA/AKT pathways and/or mutational signatures consistent with deficiency in HRD provided us with the opportunity for in vivo assessment of whether these alterations are predictive of drug response to multiple inhibitors, including 1) GS-626510 (C-MYC/BETi), 2) copanlisib (PIK3CAi), and 3) olaparib (PARPi).

Our integrated analysis results define mutated genes and pathways involved in uLMS carcinogenesis and provide a strong preclinical rationale for clinical trials targeting specific driver mutations/pathways in patients with advanced, metastatic, or recurrent uLMS.

Results

Cohort Characteristics. We analyzed the sequencing data of 83 patients with uLMS, including 56 patients recruited from Yale and 27 from The Cancer Genome Atlas (TCGA) (https://portal.gdc.cancer.gov/) Adult Soft Tissue Sarcomas study (4). The TCGA study includes a total of 27 uLMS samples, and the sequencing data were downloaded through its portal. The clinical and histological features are presented in Dataset S1. Yale and TCGA cohorts were comparable for multiple characteristics, including age ($P = 0.32$, chi-square test), number of mitosis ($P = 0.06$, chi-square test), and tumor size ($P = 0.18$, chi-square test) (Dataset S2). No difference in median overall survival (OS) was noted between the two cohorts (Yale, 45 mo vs. TCGA, 54 mo, $P = 0.629$, log-rank test) (*SI Appendix*, Fig. S1). Among the 83 included patients, WES, RNA-Seq, and WGS were performed on 82, 37, and 21 patients, respectively (Fig. 1*A*).

Genetic Landscape of uLMS. Somatic mutations were detected from 82 uLMS WES data, including 76 matched tumor-normal pairs and 6 unmatched tumors. Of these, 55 and 27 were from Yale and TCGA, respectively. Tumor and normal samples displayed a mean coverage of 154.1 and 122.9 independent sequencing reads per targeted base, respectively (Dataset S3). Of note, the TCGA cohort displayed lower sequencing coverage for both tumor and normal tissues, compared to those from Yale (Datasets S4–S6). Tumor purity was estimated as 76.4% and showed no correlation with somatic mutation burden ($R^2 = 0.15$, $P = 0.19$) (*SI Appendix*, Fig. S2). A total of 5,544 somatic variants (median = 42; range 4 to ~835) were detected, including 4,827 SNVs and 489 small insertions and deletions (Fig. 1*A* and Dataset S7). The median somatic mutation rate was 1.4 per megabase (Mb) of target sequence. The median of nonsynonymous/synonymous mutation (NS/S) ratio was 3.33, and transition/transversion (Ti/Tv) ratio was 0.98. Somatic mutation burden ($P_{wilcox} = 0.679$), NS/S ($P_{wilcox} = 0.616$), and Ti/Tv ($P_{wilcox} = 0.587$) ratios between Yale and TCGA cohorts were not significantly different (Dataset S8). We identified two patients, LMS12_1 and LEY15, which showed a high tumor mutational burden (TMB), significantly deviating from a normal distribution (Fig. 1*A*). LMS12_1 harbored a somatic frameshift deletion mutation (NM_181808: p.C734Vfs*16) in POLN, a DNA polymerase, which bypasses certain DNA lesions with genomic damage during replication (6). LEY15 carried a somatic premature termination mutation (NM_001184: p.R1503*) in ATR, a conserved DNA damage response gene. However, none of these mutations were previously reported to contribute to somatic hypermutation; thus, epigenetic factors cannot be excluded. These tumors did not display loss of heterozygosity (LOH) segments or CNVs. Neither patient had received chemotherapy prior to surgical resection. Notably, LEY15 was predicted as microsatellite instable (MSI) (score = 42.35%) when analyzed by MSIsensor2 (7), suggesting MSI plays a major role in somatic mutation accumulation (*SI Appendix*, Fig. S3). Mutational signature analysis using SigProfiler (8) on 48 fresh frozen tumor-normal pairs revealed that the homologous recombination defect (HRD; SBS3) signature was predominant in 25% of uLMS tumors. SBS3 is a mutational signature well-known to correlate with BRCA1 and BRCA2 biallelic inactivation and HRD in different solid cancers (9). We detected 12 tumors with HRD signature, of which only 4 harbored either germline or somatic mutations in homologous recombination genes. This result highlights that nearly 66.6% of tumors with predicted HRD signature cannot be authenticated as BRCA1/2 null genetically; thus, epigenetic means should be considered to validate the BRCAness. Additionally, a clear MSI/MMR (mismatch repair) signature (SBS6 or SBS21) was observed in one tumor, LEY15, which is consistent with the result from MSIsensor2. The rest of the samples were characterized by an enrichment of either clock-like aging signature (SBS1) or reactive oxygen species signature (*SI Appendix*, Fig. S4). Recurrent somatic mutations (*SI Appendix*, Fig. S5) were noted in three genes, including MED12 (NM_005120: p.G44D/V/S/R mutation in exon 2, mediator of RNA polymerase II transcription subunit 12) in six tumors (7.2%); TP53 (NM_000546: four recurrent sites; 10.8%, tumor protein P53), and PTEN (NM_000314: p.Y346* mutation; 2.4%, phosphatase and tensin homolog). The recurrent MED12 mutation has been previously reported in 7 to ~20% of uLMS (10, 11), along with many other tumors types, such as uterine leiomyoma (LM) (~70%) (11), breast fibroadenoma (59%) (12), endometrial polyps (10), and colorectal cancers (10). Two (NM_000546: pR175H and p.C238S/Y) out of four recurrent sites in TP53 have been reported as statistically significant oncogenic mutations (Q-values 0 and 7.75e−62, respectively, binomial test) in the cancer hotspot database (https://www.cancerhotspots.org/#/home) (13).

CNV in EMT Genes and TERT. We next assessed somatic CNVs in 66 matched tumors after excluding 10 matched tumors with poor DNA quality. Statistically significant focal amplified regions and deleted regions were detected using GISTIC2.0 (14) (Fig. 1*C* and Dataset S9). Chromosomes 1q21, 5p15, 8p11, 8q24, 14q11, 17p11, and 17p12 were found to be recurrently amplified (false discovery rate [FDR] < 0.25, Benjamini–Hochberg correction). The most significant focal deleted regions included known tumor suppressors, such as RB1 (13q14, 60.6%), TP53 (17p13, 30.3%), PTEN (10q23, 34.8%), CDKN2A (9p21, 22.7%), CYLD (16q12, 34.8%), BRCA2 (13q13, 34.8%), NOTCH1 (9q34, 10.6%), APC (5q31, 7.6%), and PIK3R1 (5q31, 6.1%) (2, 4, 5). A significantly amplified focal peak at 17p12, including the MAP2K4 and MYOCD genes, was detected in 30.3% (20 of 66) of the samples. Twelve patients were found to have recurrent amplifications of 8p24, which contains the C-MYC oncogene. An amplified segment in 1q21, which spans 370 genes, was present in 30 patients (45.5%). This region contains epithelial–mesenchymal transition (EMT)-associated genes S100A7, S100A8, and S100A9, which have been implicated in breast cancer recurrence and a target of pacritinib (15).

MEN1 Identified as a Driver of uLMS. In order to identify genes with an increased burden of somatic mutation, we analyzed the burden of all protein-altering somatic mutations (16). We identified

Downloaded at Palestinian Territory, occupied on November 27, 2021

www.manaraa.com

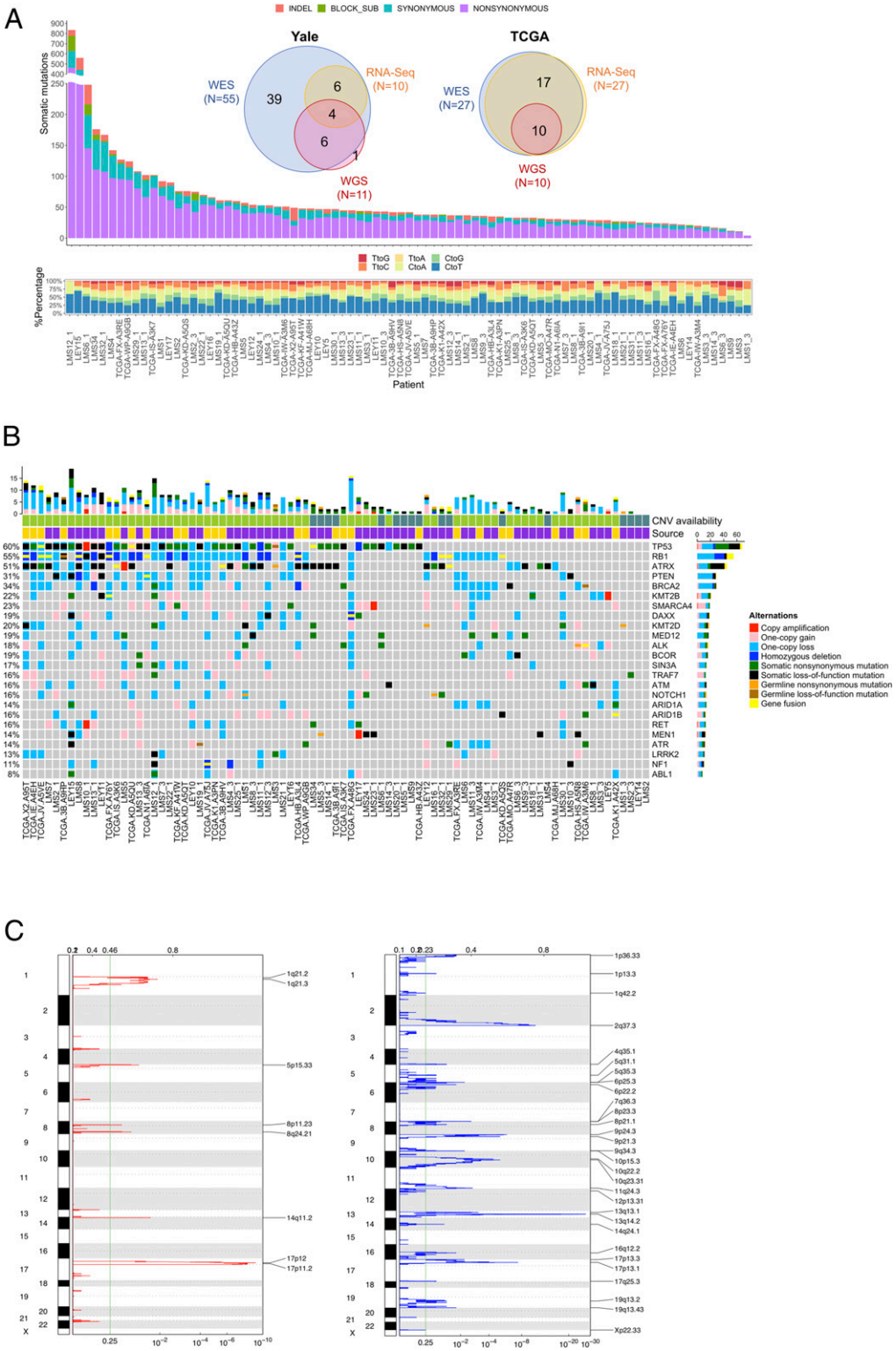

Fig. 1. Somatic mutation landscape underlying uLMS. (*A*) Venn diagram of Yale and TCGA genomic and transcriptomic data composition. Distribution of somatic mutation in 83 uLMS samples. (*B*) Frequency and type of somatic mutations. Rows represent genes affected by at least two somatic SNVs or small INDELs, and columns represent individual uLMS. Source: Yale (purple), TCGA (yellow). CNV availability: CNV data available (light green), CNV data not available (dark green). (*C*) Recurrent CNV pattern. Significant amplifications (*Left*) and deletions (*Right*). The green line indicates the cutoff for significance (q = 0.25).

Downloaded at Palestinian Territory, occupied on November 27, 2021

www.manaraa.com

four significantly mutated genes with a genome-wide FDR of 0.1 (Fig. 2*A* and Dataset S10). While three of these have been previously reported uLMS drivers (2–4, 17), including TP53 (43.9%), ATRX (30.4%), and PTEN (4.9%), the driver MEN1 (6.1%) has also been identified. MEN1 harbored loss of function (LoF) somatic mutations in five patients and a germline missense mutation predicted as deleterious by MetaSVM (18) in one patient, LMS5_3 (Fig. 2*B*). MEN1 functions as an essential component of an MLL/SET1 histone methyltransferase (HMT) complex, which methylates "Lys-4" of histone H3 (H3K4) and has been shown to bind to the TERT promoter repressing telomerase expression (19, 20). To confirm that these were LoF events, we analyzed RNA-Seq data on 37 available patients. Patients with MEN1 alterations showed a significantly reduced expression compared with noncarriers ($P_{adj} = 7.81 \times 10^{-3}$, negative binomial test) (*SI Appendix*, Fig. S6*B*). We further noted that MEN1 is relatively highly expressed in the uterus according to GTEx V8 (https://gtexportal.org/home/, median TPM = 31.85) (*SI Appendix*, Fig. S6*A*). As MEN1 is associated with multiple endocrine neoplasia 1 syndrome and 1 to 7% of MEN1 patients present LMs (21) or LMSs (22–24), our results provide evidence for a link between MEN1 alterations and uLMS. TP53 was the most frequently mutated gene for somatic SNVs and small insertions/deletions (INDELs) (36 of 83) in addition to CNVs (16 of 66) (Fig. 1*B*). As previously described using mouse models, TP53 mutations may result in either LoF or gain-of-function promoting tumorigenesis (25, 26). The expression data also did not show significant changes among mutation carriers and noncarriers (*SI Appendix*, Fig. S6*B*). TP53 mutations trend toward decreased survival rate ($P = 0.051$, log-rank test) (Fig. 2*C*). Furthermore, 25 out of 83 patients carry ATRX somatic mutations, and 24.2% of uLMS tumors display CNVs. ATRX is a tumor suppressor gene involved in transcriptional regulation that has previously been implicated in both uLMS and soft tissue LMS (STLMS) (4). RNA expression results between ATRX mutation carriers and noncarriers confirmed that the detected alterations result in decreased gene expression ($P_{adj} = 0.036$, negative binomial test) (*SI Appendix*, Fig. S6) and are significantly associated with decreased survival ($P = 0.001$, log-rank test) (Fig. 2*C* and *SI Appendix*, Fig. S7). ATRX and its partner protein, DAXX, form the H3.3 chaperone, which has previously been demonstrated to regulate ALT (27–29). Of note, we detected three tumors harboring DAXX somatic alterations—mutually exclusive for ATRX alterations (Fig. 1*B*).

Fusion and Simple Structural Variations in uLMS. Analysis of RNA-Seq revealed 833 fusions in 37 uLMS samples, with an average of

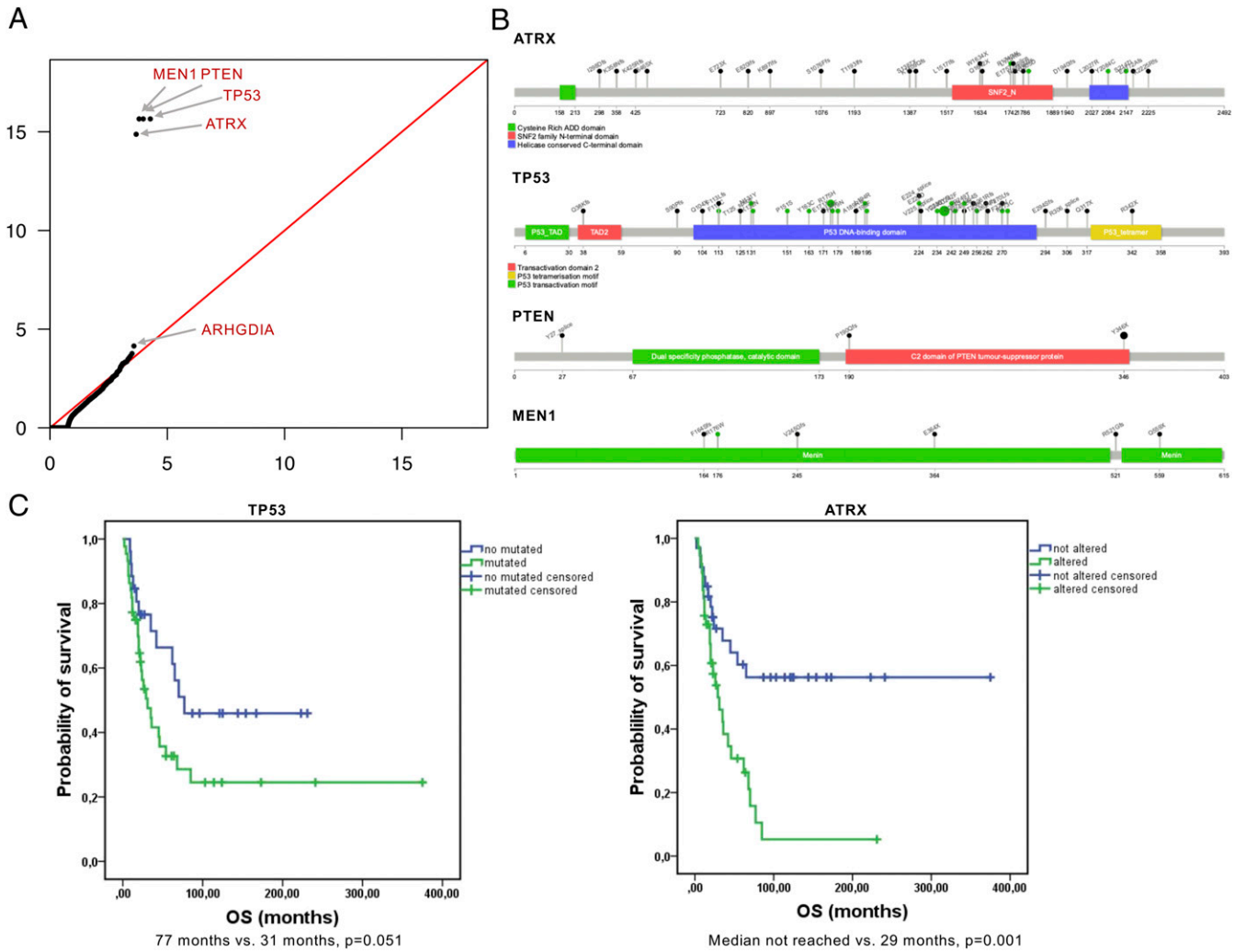

Fig. 2. Mutational gene burden in uLMS. (*A*) Q–Q plot of significantly mutated genes according to MutSigCV. (*B*) Schematic representation of SNVs and INDELs in significantly mutated genes MEN1, TP53, ATRX, and PTEN using Lollipops tool (https://github.com/joiningdata/lollipops). (*C*) Kaplan–Meier curves comparing overall survival according to TP53 (77 mo vs. 31 mo, $P = 0.051$) mutation and ATRX status (median not reached vs. 29 mo, $P = 0.001$).

Downloaded at Palestinian Territory, occupied on November 27, 2021

www.manaraa.com

22.5 events per sample (37.0 per Yale sample and 17.1 per TCGA sample). Among them, two known fusion events (i.e., ACTG2-ALK and KAT6B-KANSL1) were reported in LMS (30) and LM (31, 32), respectively (Fig. 3*A*). The KAT6B-KANSL1 event results in the fusion connecting the NEMM domain of KAT8 and the PEHE domain of KANSL1. The fusion protein has been shown to have a high affinity to chromatin and transcription regulation (31). The ACTG2-ALK fusion event includes an ACTG2 promoter, which is highly expressed in the smooth muscle cell, and ALK, a protein tyrosine kinase domain (30). We posit this may result in driving a high expression of tyrosine kinase in the myometrium. Additionally, multiple rearrangements were observed disrupting LMS driver genes, including RB1, TP53, ATRX, and DAXX. Ten (27.0%) samples harbor RB1 fusions (Dataset S11). Most of the break points locate around RB1's DUF3452 and RB_A domains, likely resulting in the truncation of RB1 protein (Fig. 3*B*). Similarly, 3 (8.1%), 3 (8.1%), and 1 (2.7%) samples carry fusion/translocation disrupting TP53, ATRX, and DAXX, respectively. We also observed that known tumor suppressor genes, such as CAMTA1, SETD2, and KDM5C, were disrupted in more than one sample (Dataset S11). These data support the view that somatic structural variations in these tumor suppressor genes (RB1, TP53, ATRX, DAXX, CAMTA1, SETD2, KDM5C) may represent one of the critical mechanisms for driving tumorigenesis in uLMS and, accordingly, may explain ~43.2% (16 of 37) of cases. Furthermore, assuming that many of the known causal fusion events may drive the expression of oncogenes, we restricted the fusion gene analysis to oncogenes based on OncoKB (33). After examining the direction of the fusions, eight potential oncogenic fusion events were identified (Dataset S11). Additionally, WES analysis revealed 323 structural variations (translocations, inversions, deletions, duplications) in 76 paired uLMS samples (Dataset S12). Twenty-six events covered known cancer genes, including a deletion within ATRX and an additional inversion encompassing TP53.

Complex Structural Variations in uLMS. Multiple complex structural variations were detected from 21 uLMS samples (11 Yale samples and 10 TCGA samples) by analyzing WGS data using JaBbA, which infers junction balanced cancer genome graphs with mixed-integer programming of read depth and junctions (Fig. 4*A*) (34). Among them, 16 out of 21 (76.2%) samples harbor chromoplexy/chromothripsis (Fig. 4*B*). RB1 copy loss and fusion were observed in the chromoplexy/chromothripsis region of 4 samples (Fig. 4*C*), indicating that chromoplexy/chromothripsis might result in the ultimate LoF of RB1 in uLMS. Other complex events include 18 with tic (templated insertion chains), 4 with pyrgo (accumulated tandem duplications), 5 with dm (double minute or extrachromosomal circular DNA), and 7 with rigma (accumulated simple deletions) (Fig. 4*A*).

PARP, C-MYC/BET, and PIK3CA Inhibitors Are Active In Vivo against uLMS PDXs. Since 25% (12 of 48) of the fresh frozen uLMS harbored an HRD signature, 18.2% (12 of 66) demonstrated C-MYC amplification, and 61.4% (51 of 83) harbored an alteration in PTEN/PIK3CA/AKT/mTOR genes, we took advantage of two recently established uLMS PDXs (i.e., LEY11 and LEY16) harboring gain of function in C-MYC, PTEN mutations and/or HRD signatures (Fig. 5 and Datasets S14 and S15) to evaluate the activity of olaparib (Astra Zeneca), a PARPi approved by the Food and Drug Administration (FDA) for the treatment of HRD-positive ovarian cancer patients, among other solid tumors; copanlisib (Bayer Pharmaceuticals Inc), an intravenous, selective pan-Class I PI3K inhibitor highly active in PIK3CA mutant tumors approved by the FDA for the treatment of patients with relapsed follicular lymphoma; and GS-626510

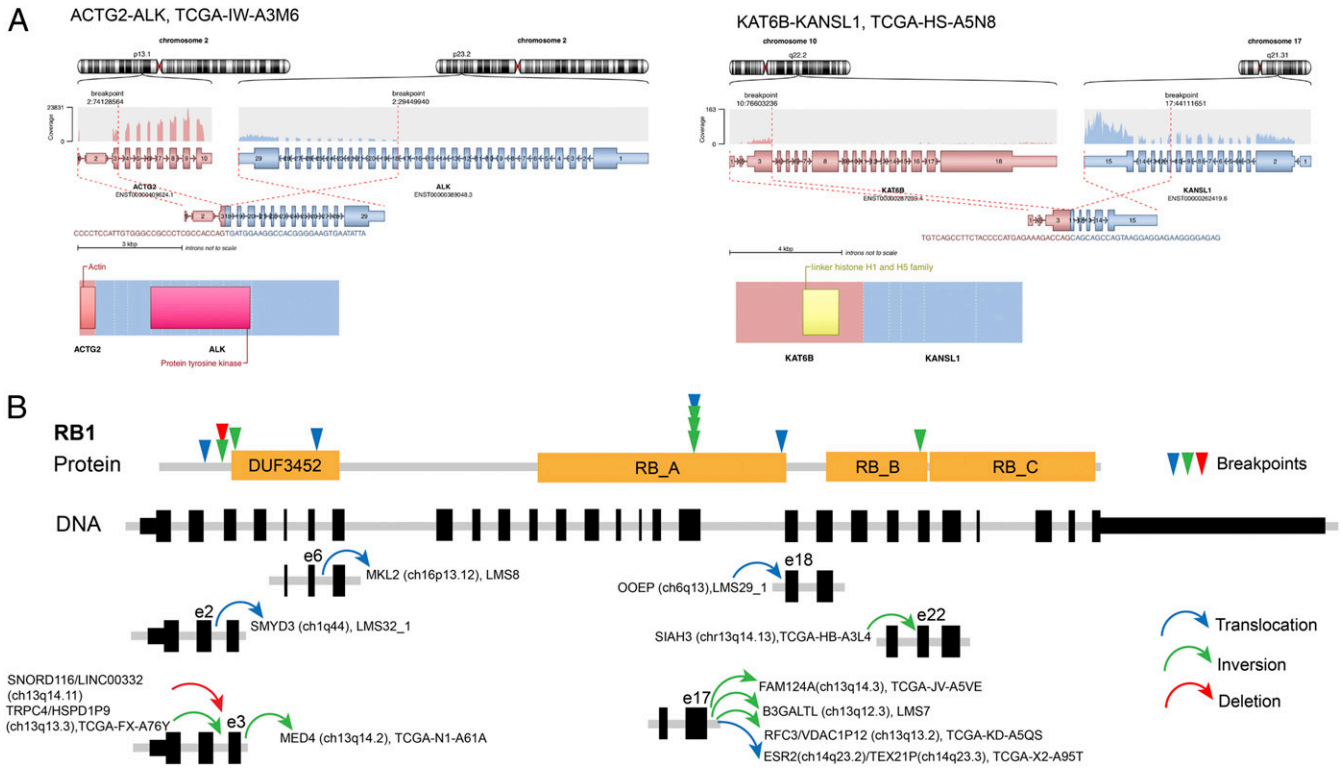

Fig. 3. Fusions and translocations in uLMS. (*A*) ACTG2-ALK and KAT6B-KANSL1 fusions detected in TCGA-IW-A3M6 and TCGA-HS-A5N8, respectively. (*B*) Fusions detected in RB1 in 10 uLMS samples. (*Upper*) Protein domains of RB1. Triangle arrows indicate the break points. (*Bottom*) Exon distributions of RB1. Curved arrows indicate different types of fusion events.

Downloaded at Palestinian Territory, occupied on November 27, 2021

www.manaraa.com

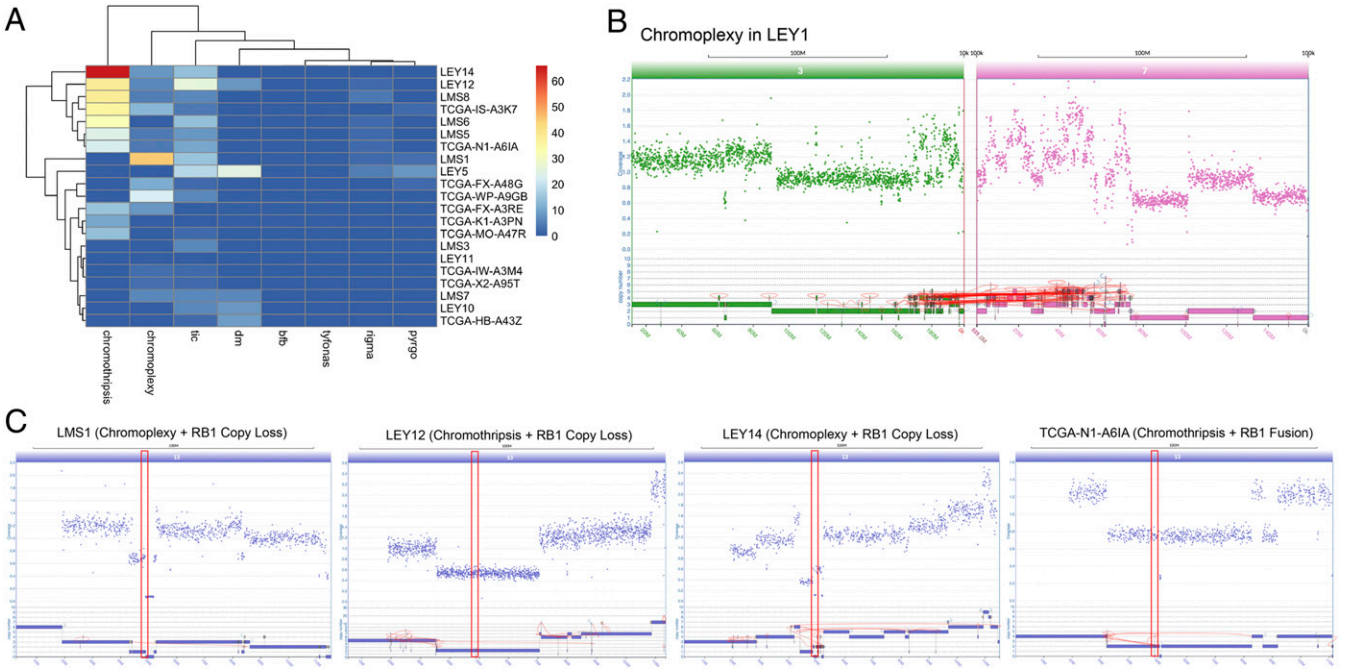

Fig. 4. Complex structural variations in 21 μLMS samples with WGS. (*A*) Heat map of different types of complex structural variation events across 21 samples. The color bar indicates the number of junctions. (*B*) An example of a chromoplexy event found in LEY1. (*C*) Chromoplexy/chromothripsis events that potentially lead to RB1 copy loss in four μLMS samples.

(Gilead Sciences Inc.), a novel BET bromodomain inhibitor currently in clinical trials. We found olaparib, copanlisib, and GS-626510 to be able to significantly inhibit tumor growth when compared to vehicle-treated mice in both PDX models. Indeed, as shown for the LEY11 PDX in Fig. 5*A*, mice undergoing copanlisib (5 mg/kg once a day [QD]) and GS-626510 (10 mg/kg twice a day [BID]) treatment for a total of 13 d demonstrated a significantly slower rate of tumor growth compared to vehicle control animals ($P = 0.0001$ and $P < 0.000001$, respectively). Similarly, mice treated with a twice-daily oral treatment with olaparib (50 mg/kg) exhibited a significantly slower rate of tumor growth compared with vehicle control in the LEY16 PDX model (Fig. 5*B*). This difference was statistically significant starting on dosing day 25 ($P = 0.002$). Likewise, mice harboring LEY16 and undergoing daily treatment with GS-626510 (10 mg/kg) exhibited a significantly slower rate of tumor growth when compared to control-treated mice ($P = 0.0005$) (Fig. 5*C*).

Discussion

We report the whole-genome, whole-exome, and RNA-Seq characteristics of a large cohort of uLMS. These integrated results define the genetic hallmarks of this highly aggressive variant of uterine sarcoma and identify multiple mutated genes and deranged pathways potentially targetable with currently available therapeutic drugs.

Using WES, we found uLMS to harbor mutations in well-recognized cancer genes, including TP53 (altered in 60%), RB1 (altered in 55%), and PTEN (altered in 31%). These data are in agreement with previous studies in LMS (2, 4) and support

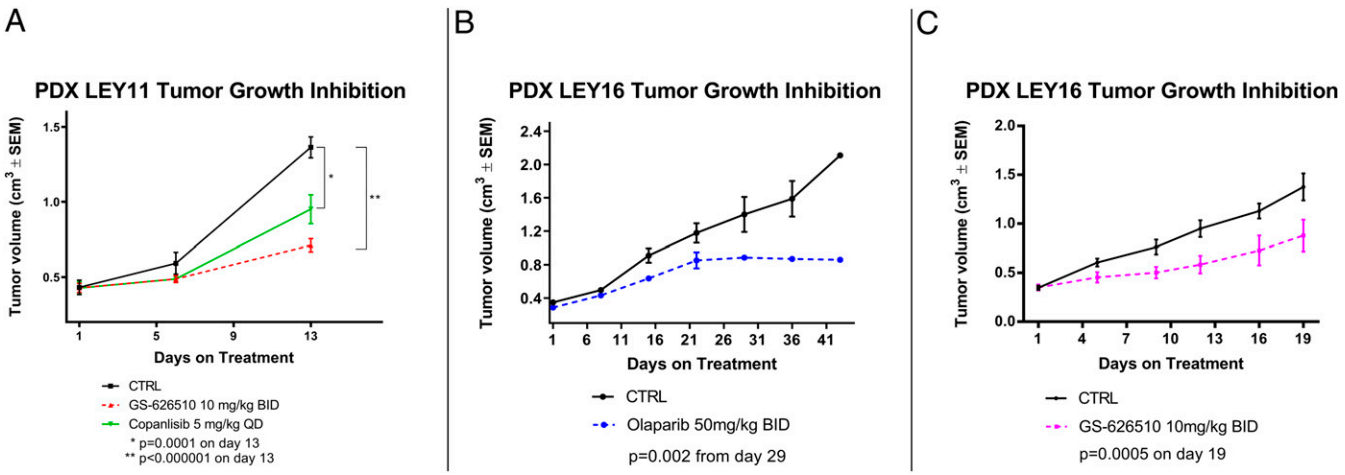

Fig. 5. Copanlisib, Olaparib, and GS-626510 inhibited cell proliferation in uLMS PDXs in vivo. (*A*) Copanlisib and GS-626510 tumor growth inhibition in LEY11. (*B* and *C*) Olaparib and GS-626510 tumor growth inhibition in LEY16.

Downloaded at Palestinian Territory, occupied on November 27, 2021

www.manaraa.com

the notion that inactivation of these well-established tumor suppressor genes plays an important role in uLMS carcinogenesis. Alterations in ATRX, a gene encoding a transcriptional regulator that contains an ATPase/helicase domain, and a member of the SWI/SNF family of chromatin remodeling proteins, were also detected in 51% of uLMS. ATRX is known to functionally cooperate with DAXX, a gene we also found mutated in 19% of uLMS. Importantly, when we investigated RNA levels between ATRX/DAXX mutation carriers and noncarriers, we confirmed the detected alterations resulted in decreased gene expression, a finding associated with ALT, which is a telomerase-independent mechanism found in mesenchymal tumors that often activates for tumors to achieve replicative immortality (27–29, 35). Notably, patients with ATRX/DAXX mutations were characterized by a significantly shorter survival, supporting the view that alterations in this DNA repair pathway trigger a more aggressive uLMS phenotype (*SI Appendix*, Fig. S7). These findings may have important clinical implications since they may allow the triage of uLMS patients in different risk categories and potentially guide adjuvant treatment. More importantly, ATRX/DAXX mutations have recently demonstrated to render cancer cells hypersensitive to ATR inhibitors (36–38). Accordingly, these data suggest that novel ATR inhibitors currently in clinical trials (for example BAY1895344, Bayer) may represent new, potentially effective treatment options for the large (60.2% in our series) subset of patients with advanced/recurrent uLMS carrying ATRX/DAXX mutations. Another gene of interest was MED12, a gene commonly mutated in uterine LMs and encoding a subunit of the Mediator complex which can both repress and activate gene transcription (3, 10, 39). While the role of MED12 mutations in uLMS remains poorly understood, our data highlight an oncogenic mechanism shared by both uterine LM and a subset of uLMS. However, whether the small subsets of uLMS harboring MED12 mutations (7.2%) stem from dedifferentiated uterine LMs, as previously claimed (11), remains unproven. Importantly, we also identified a significant increase in somatic mutations in MEN1, a gene to our knowledge not yet implicated in uLMS. Specifically, MEN1 somatic deletions or SNVs were found in 6.1% (4 of 66) and 6.0% (5 of 83) of uLMS, respectively. MEN1 is associated with multiple endocrine neoplasia 1 syndrome, and it is known to play a key role in the MLL/SET1 HMT complex, which methylates "Lys-4" of histone H3 (H3K4) and binds to the TERT promoter repressing telomerase expression (19–21). Based on our RNA-Seq analysis, MEN1 somatic SNV/CNV alterations resulted in a loss of MEN1 expression (*SI Appendix*, Fig. S6). Taken together, these findings support the notion that MEN1 gene somatic loss-of-function alterations may play an important role in the tumorigenesis of a subset of uLMS (8 of 83). Alterations in PTEN, a negative regulator of the PI3KCA/AKT/mTOR signaling pathway, were detected in 31% of uLMS while derangement in the PIK3CA/AKT/mTOR pathway, which is known to play an important role in multiple cancer-related processes including but not limited to cell growth and resistance to chemotherapy (40, 41), were detected in 51 of uLMS. Notably, multiple PIK3CA inhibitors have recently been approved clinically for the treatment of both solid and liquid human cancers and, accordingly, may potentially represent novel therapeutic tools for the treatment of chemotherapy-resistant/metastatic uLMS. Consistent with this hypothesis, our group has recently demonstrated the preclinical activity of various Her2/neu/PIK3CA/AKT/mTOR inhibitors against carcinosarcomas, another biologically aggressive uterine tumor (42).

The number and type of somatic mutations (i.e., mutational signatures) extracted from WES data are known to vary widely between cancer types since they are the consequence of multiple mutational processes. Importantly, we detected enrichment of three known mutational signatures, including defective DNA repair (i.e., HRD, altered in 25%) and MMR (i.e., MSI altered in 2%), which are potentially targetable with currently available agents. Indeed, the finding that MMR-defective MSI-H human cancers may respond favorably to immune checkpoint inhibitors (43), regardless of the organ of origin, raises the question of whether the same applies to uLMS with a hypermutator phenotype.

Using CNV analysis, we identified several cancer driver genes that possibly contribute to uLMS. In this regard, the most significant focal deleted regions included known tumor suppressor genes, such as RB1, TP53, PTEN, and BRCA2 genes, while frequent amplifications were identified in some well-known cancer genes, such as C-MYC (12 of 66, 18.2%), TERT (17 of 66, 25.8%), MAP2K4 (20 of 66, 30.3%), and MYOCD (23 of 66, 34.8%) (2, 4, 5). Of interest, both the MYOCD gene, a transcriptional cofactor of serum response factor (SRF) regulating smooth muscle development and differentiation (44), and the mitogen-activated protein kinase kinase 4 (MAP2K4) gene, a member of the mitogen-activated protein kinase (MAPK) activator family, are known to play a significant role in cell proliferation, differentiation, and transcriptional regulation and have previously been demonstrated to promote tumor cell migration and metastases (44, 45) (i.e., the main cause of death of uLMS patients). Importantly, MAP2K4 inhibitors such as PLX8725 (Plexxikon) are currently entering phase I clinical trials and might therefore represent additional therapeutic tools to target chemotherapy-resistant uLMS.

Given the frequency of c-MYC amplification, the common derangement of the PI3K/AKT/mTOR pathway, and the prevalence of the WES-extracted mutational signature consistent with HRD in uLMS, we took advantage of two recently established and fully sequenced PDXs to evaluate whether these alterations are predictive of drug response to GS626510 (an orally bioavailable Bromodomain and Extra-Terminal motif [BET]/C-MYCi), copanlisib (a PIK3CAi), and olaparib (a PARPi). We showed that GS-626510 has significant inhibitory activity against both the LEY11 and LEY16 PDX models. These encouraging preclinical data with GS-626510 in uLMS xenografts confirm and expand the results of our recent work targeting c-MYC gain of function in chemotherapy-resistant ovarian tumors (46). Copanlisib, a PIK3CA inhibitor administered intravenously, was also found to be significantly active in controlling the growth of the LEY11 xenografts harboring a deranged PTEN/PI3K/AKT/mTOR pathway. Finally, olaparib, a PARPi indicated for the treatment of multiple human tumors characterized by "BRCAness" and/or platinum sensitivity, demonstrated significant activity in the signature 3 (i.e., HRD) enriched LEY16 PDX model. Collectively, our preclinical in vivo validation results suggest that a large subset of uLMS unresponsive to chemotherapy might potentially benefit from existing PTEN/PIK3CA/PARP/C-MYC/BET-targeted drugs, as well as other novel targeted agents attacking additional deranged pathways identified in our cohort (*SI Appendix*, Fig. S8). Finally, to discover putative gene fusions, we analyzed transcriptomic data from 37 uLMS samples. We found frequent fusions disrupting RB1, TP53, ATRX/DAXX, CAMTA1, SETD2, and KDM5C genes. Clinically important fusion events, including oncogenic ALK fusions (ACTG2-ALK) potentially responsive to ALK inhibitors (for example, crizotinib/lorlatinib/ceritinib), were called, suggesting a small subset of uLMS may also harbor actionable kinase gene translocations (30). Using WGS, we found the majority of uLMS to harbor complex karyotypes, with over two-thirds of the tumor samples found to harbor chromoplexy and/or chromothripsis.

In conclusion, our integrated whole-genome, whole-exome, and RNA-Seq results defined the genetic landscape of uLMS and identified multiple potentially actionable deranged genes/pathways. Since advanced/recurrent and/or metastatic uLMS remain incurable, our comprehensive genetic results, combined with our preclinical validation data using PDXs, strongly suggest that HRD, ERBB2/PI3K/AKT/mTOR, and C-MYC/BET

Downloaded at Palestinian Territory, occupied on November 27, 2021

www.manaraa.com

deranged pathways may be clinically susceptible to targeted inhibitors in a large subset of uLMS. These findings will help guide further research and targeted therapies against this highly lethal cancer worldwide.

Material and Methods

Patient and Specimen Acquisition. The study protocol was approved by the Yale Human Investigation Committee and by the Research Review Board-Ethic Committee of the Azienda Socio Sanitaria Territoriale (ASST) Spedali Civili, Brescia, Italy (study reference number: NP1284) and was conducted in accordance with the Declaration of Helsinki. Informed consent from the participant and/or her legally authorized representative (surrogate) was obtained prior to initiating any research activities. DNA and/or RNA was extracted from a total of 23 fresh frozen uLMS, including two PDXs and 33 formalin-fixed paraffin-embedded (FFPE) tumor blocks from patients with uLMS, who underwent staging at the Yale New Haven Hospital, the University of Arkansas for Medical Sciences (UAMS) (Little Rock, AR), and at the ASST Spedali Civili di Brescia/University of Brescia, Brescia, Italy.

WES and Analysis. Genomic DNA from 55 Yale tumor samples together with 49 matched normal tissues were sent for WES. The sequencing data were processed using the GATK Best Practice workflow (47–49). After determining tumor purity, somatic SNVs were called using GATK4 MuTect2 (50), and INDELs were called using the intersection of the two callers MuTect2 and Strelka2 (51) for tumor-normal paired tissues, and, for unmatched tumors, the intersection of MuTect2 and Pisces (52) was used. Gene burden analysis was performed using MutSigCV (16). Mutational matrices were constructed using SigProfilerMatrixGenerator (53), and mutational signatures were extracted using SigProfiler (8). See *SI Appendix, Materials, and Methods* for details.

Somatic CNV Analysis. Somatic CNVs were called from paired samples with WES using EXCAVATOR (54), and enrichment analysis was performed using GISTIC2.0 (14) (see *SI Appendix, Materials and Methods* for details).

Transcriptome Sequencing and Analysis. Ten uLMS samples were subjected to RNA-Seq. Sequencing reads were aligned and processed using HISAT2 (55) and HTSeq-count (56). Gene differential expression was analyzed using DESeq2 (57). See *SI Appendix, Materials and Methods* for details.

Fusion and Simple Structural Variation Analysis. Fusion events were detected from 37 RNA-Seq samples using Arriba (https://github.com/suhrig/arriba/) and STAR-fusion (58). Structural variations were also called from 76 WES samples using DELLY2 (59), Manta (60), and SvABA (61) (see *SI Appendix, Materials and Methods* for details).

WGS and Analysis. Eleven uLMS samples were subjected to WGS. JaBbA (Junction balanced analysis, https://github.com/mskilab/JaBbA) (34) was used to reconstruct cancer genome graphs (see *SI Appendix, Materials and Methods* for details).

Xenograft Implantation and In Vivo Drug Study. Briefly, the LEY11 and LEY16 PDX were xenografted in female CB17/lcrHsd-Prkd/scid mice subcutaneously into the lower abdomen area. Mice were triaged into treatment groups when the tumor was established. Dosing began upon reaching target size and was delivered intravenously daily for Copanlisib and orally BID for Olaparib and GS-626510 for a total of 43 or 20 d, respectively. After the last dose administration, animals were either euthanized or followed for survival. All mice were housed and treated in accordance with the policies set forth by the Institutional Animal Care and Use Committee (IACUC) at Yale University.

Data Availability. All study data are included in the article and/or supporting information.

ACKNOWLEDGMENTS. This work was supported in part by Gilead Sciences Inc. (Foster City, CA), U01 CA176067-01A1 grants from NIH, the Deborah Bunn Alley Foundation, the Tina Brozman Foundation, the Discovery to Cure Foundation, and the Guido Berlucchi Foundation (to A.D.S.). This investigation was also supported by NIH Research Grant CA-16359 from the National Cancer Institute and by Stand Up To Cancer (SU2C) Convergence Grant 2.0 (to A.D.S.). This work was also supported by a Korea University Medical Center Grant. A.M. was supported by a fellowship from the Spanish Society of Medical Oncology. W.D. was supported by American Heart Association Predoctoral Fellowship 19PRE34380842.

1. F. Amant, A. Coosemans, M. Debiec-Rychter, D. Timmerman, I. Vergote, Clinical management of uterine sarcomas. *Lancet Oncol.* **10**, 1188–1198 (2009).
2. P. Chudasama *et al.*, Integrative genomic and transcriptomic analysis of leiomyosarcoma. *Nat. Commun.* **9**, 144 (2018).
3. N. Mäkinen *et al.*, Exome sequencing of uterine leiomyosarcomas identifies frequent mutations in TP53, ATRX, and MED12. *PLoS Genet.* **12**, e1005850 (2016).
4. Cancer Genome Atlas Research Network. Electronic address: elizabeth.demicco@sinaihealthsystem.ca; Cancer Genome Atlas Research Network, Comprehensive and integrated genomic characterization of adult soft tissue sarcomas. *Cell* **171**, 950–965.e28 (2017).
5. T. Cuppens *et al.*, Integrated genome analysis of uterine leiomyosarcoma to identify novel driver genes and targetable pathways. *Int. J. Cancer* **142**, 1230–1243 (2018).
6. G. L. Moldovan *et al.*, DNA polymerase POLN participates in cross-link repair and homologous recombination. *Mol. Cell. Biol.* **30**, 1088–1096 (2010).
7. B. Niu *et al.*, MSIsensor: Microsatellite instability detection using paired tumor-normal sequence data. *Bioinformatics* **30**, 1015–1016 (2014).
8. L. B. Alexandrov *et al.*; PCAWG Mutational Signatures Working Group; PCAWG Consortium, The repertoire of mutational signatures in human cancer. *Nature* **578**, 94–101 (2020).
9. P. Polak *et al.*, A mutational signature reveals alterations underlying deficient homologous recombination repair in breast cancer. *Nat. Genet.* **49**, 1476–1486 (2017).
10. K. Kämpjärvi *et al.*, Somatic MED12 mutations in uterine leiomyosarcoma and colorectal cancer. *Br. J. Cancer* **107**, 1761–1765 (2012).
11. G. Ravegnini *et al.*, MED12 mutations in leiomyosarcoma and extrauterine leiomyoma. *Mod. Pathol.* **26**, 743–749 (2013).
12. S. Piscuoglio *et al.*, MED12 somatic mutations in fibroadenomas and phyllodes tumours of the breast. *Histopathology* **67**, 719–729 (2015).
13. M. T. Chang *et al.*, Accelerating discovery of functional mutant alleles in cancer. *Cancer Discov.* **8**, 174–183 (2018).
14. C. H. Mermel *et al.*, GISTIC2.0 facilitates sensitive and confident localization of the targets of focal somatic copy-number alteration in human cancers. *Genome Biol.* **12**, R41 (2011).
15. J. Y. Goh *et al.*, Chromosome 1q21.3 amplification is a trackable biomarker and actionable target for breast cancer recurrence. *Nat. Med.* **23**, 1319–1330 (2017).
16. M. S. Lawrence *et al.*, Mutational heterogeneity in cancer and the search for new cancer-associated genes. *Nature* **499**, 214–218 (2013).
17. C. Y. Yang *et al.*, Targeted next-generation sequencing of cancer genes identified frequent TP53 and ATRX mutations in leiomyosarcoma. *Am. J. Transl. Res.* **7**, 2072–2081 (2015).
18. C. Dong *et al.*, Comparison and integration of deleteriousness prediction methods for nonsynonymous SNVs in whole exome sequencing studies. *Hum. Mol. Genet.* **24**, 2125–2137 (2015).
19. K. Suphapeetiporn, J. M. Greally, D. Walpita, T. Ashley, A. E. Bale, MEN1 tumor-suppressor protein localizes to telomeres during meiosis. *Genes Chromosomes Cancer* **35**, 81–85 (2002).
20. M. Hashimoto *et al.*, Role of menin in the regulation of telomerase activity in normal and cancer cells. *Int. J. Oncol.* **33**, 333–340 (2008).
21. H. Choi *et al.*, Multiple endocrine neoplasia type 1 with multiple leiomyomas linked to a novel mutation in the MEN1 gene. *Yonsei Med. J.* **49**, 655–661 (2008).
22. F. Gibril *et al.*, Prospective study of thymic carcinoids in patients with multiple endocrine neoplasia type 1. *J. Clin. Endocrinol. Metab.* **88**, 1066–1081 (2003).
23. S. Marx *et al.*, Multiple endocrine neoplasia type 1: Clinical and genetic topics. *Ann. Intern. Med.* **129**, 484–494 (1998).
24. H. Raef *et al.*, A novel deletion of the MEN1 gene in a large family of multiple endocrine neoplasia type 1 (MEN1) with aggressive phenotype. *Clin. Endocrinol. (Oxf.)* **75**, 791–800 (2011).
25. M. Oren, V. Rotter, Mutant p53 gain-of-function in cancer. *Cold Spring Harb. Perspect. Biol.* **2**, a001107 (2010).
26. G. A. Lang *et al.*, Gain of function of a p53 hot spot mutation in a mouse model of Li-Fraumeni syndrome. *Cell* **119**, 861–872 (2004).
27. T. V. Ahvenainen *et al.*, Loss of ATRX/DAXX expression and alternative lengthening of telomeres in uterine leiomyomas. *Cancer* **124**, 4650–4656 (2018).
28. R. F. de Wilde *et al.*, Loss of ATRX or DAXX expression and concomitant acquisition of the alternative lengthening of telomeres phenotype are late events in a small subset of MEN-1 syndrome pancreatic neuroendocrine tumors. *Mod. Pathol.* **25**, 1033–1039 (2012).
29. A. D. Singhi *et al.*, Alternative lengthening of telomeres and loss of DAXX/ATRX expression predicts metastatic disease and poor survival in patients with pancreatic neuroendocrine tumors. *Clin. Cancer Res.* **23**, 600–609 (2017).
30. L. E. Davis *et al.*, Discovery and characterization of recurrent, targetable ALK fusions in leiomyosarcoma. *Mol. Cancer Res.* **17**, 676–685 (2019).
31. I. Panagopoulos, L. Gorunova, B. Bjerkehagen, S. Heim, Novel KAT6B-KANSL1 fusion gene identified by RNA sequencing in retroperitoneal leiomyoma with t(10;17)(q22; q21). *PLoS One* **10**, e0117010 (2015).
32. A. J. Ainsworth *et al.*, Leiomyoma with KAT6B-KANSL1 fusion: Case report of a rapidly enlarging uterine mass in a postmenopausal woman. *Diagn. Pathol.* **14**, 32 (2019).
33. D. Chakravarty *et al.*, OncoKB: A precision oncology knowledge base. *JCO Precis. Oncol.* **2017**, PO.17.00011 (2017).

Downloaded at Palestinian Territory, occupied on November 27, 2021

www.manaraa.com

34. K. Hadi *et al*., Distinct classes of complex structural variation uncovered across thousands of cancer genome graphs. *Cell* **183**, 197–210.e32 (2020).
35. C. J. VandenBussche *et al*., Alternative lengthening of telomeres and ATRX/DAXX loss can be reliably detected in FNAs of pancreatic neuroendocrine tumors. *Cancer Cytopathol.* **125**, 544–551 (2017).
36. J. P. Amorim, G. Santos, J. Vinagre, P. Soares, The role of ATRX in the alternative lengthening of telomeres (ALT) phenotype. *Genes (Basel)* **7**, 66 (2016).
37. M. A. Dyer, Z. A. Qadeer, D. Valle-Garcia, E. Bernstein, ATRX and DAXX: Mechanisms and mutations. *Cold Spring Harb. Perspect. Med.* **7**, a026567 (2017).
38. Y. Hu *et al*., Switch telomerase to ALT mechanism by inducing telomeric DNA damages and dysfunction of ATRX and DAXX. *Sci. Rep.* **6**, 32280 (2016).
39. E. Bertsch *et al*., MED12 and HMGA2 mutations: Two independent genetic events in uterine leiomyoma and leiomyosarcoma. *Mod. Pathol.* **27**, 1144–1153 (2014).
40. K. K. Brown, A. Toker, The phosphoinositide 3-kinase pathway and therapy resistance in cancer. *F1000Prime Rep.* **7**, 13 (2015).
41. E. Paplomata, R. O'Regan, New and emerging treatments for estrogen receptor-positive breast cancer: Focus on everolimus. *Ther. Clin. Risk Manag.* **9**, 27–36 (2013).
42. C. Han *et al*., Novel targeted therapies in ovarian and uterine carcinosarcomas. *Discov. Med.* **25**, 309–319 (2018).
43. N. J. Llosa *et al*., The vigorous immune microenvironment of microsatellite instable colon cancer is balanced by multiple counter-inhibitory checkpoints. *Cancer Discov.* **5**, 43–51 (2015).
44. G. Pérot *et al*., Strong smooth muscle differentiation is dependent on myocardin gene amplification in most human retroperitoneal leiomyosarcomas. *Cancer Res.* **69**, 2269–2278 (2009).
45. J. M. Pavese *et al*., Mitogen-activated protein kinase kinase 4 (MAP2K4) promotes human prostate cancer metastasis. *PLoS One* **9**, e102289 (2014).
46. C. Li *et al*., Mutational landscape of primary, metastatic, and recurrent ovarian cancer reveals c-MYC gains as potential target for BET inhibitors. *Proc. Natl. Acad. Sci. U.S.A.* **116**, 619–624 (2019).
47. A. McKenna *et al*., The genome analysis toolkit: A MapReduce framework for analyzing next-generation DNA sequencing data. *Genome Res.* **20**, 1297–1303 (2010).
48. G. A. Van der Auwera *et al*., From FastQ data to high confidence variant calls: The genome analysis toolkit best practices pipeline. *Curr. Protoc. Bioinformatics* **43**, 11.10.1–11.10.33 (2013).
49. A. Auton *et al*.; 1000 Genomes Project Consortium, A global reference for human genetic variation. *Nature* **526**, 68–74 (2015).
50. D. Benjamin *et al*., Calling somatic SNVs and indels with Mutect2. *bioRxiv* [Preprint] (2019). https://doi.org/10.1101/861054 (Accessed 28 November 2020).
51. S. Kim *et al*., Strelka2: Fast and accurate calling of germline and somatic variants. *Nat. Methods* **15**, 591–594 (2018).
52. T. Dunn *et al*., Pisces: An accurate and versatile variant caller for somatic and germline next-generation sequencing data. *Bioinformatics* **35**, 1579–1581 (2019).
53. E. N. Bergstrom *et al*., SigProfilerMatrixGenerator: A tool for visualizing and exploring patterns of small mutational events. *BMC Genomics* **20**, 685 (2019).
54. A. Magi *et al*., EXCAVATOR: Detecting copy number variants from whole-exome sequencing data. *Genome Biol.* **14**, R120 (2013).
55. M. Pertea, D. Kim, G. M. Pertea, J. T. Leek, S. L. Salzberg, Transcript-level expression analysis of RNA-seq experiments with HISAT, StringTie and Ballgown. *Nat. Protoc.* **11**, 1650–1667 (2016).
56. S. Anders, P. T. Pyl, W. Huber, HTSeq–A Python framework to work with high-throughput sequencing data. *Bioinformatics* **31**, 166–169 (2015).
57. M. I. Love, W. Huber, S. Anders, Moderated estimation of fold change and dispersion for RNA-seq data with DESeq2. *Genome Biol.* **15**, 550 (2014).
58. B. J. Haas *et al*., Accuracy assessment of fusion transcript detection via read-mapping and de novo fusion transcript assembly-based methods. *Genome Biol.* **20**, 213 (2019).
59. T. Rausch *et al*., DELLY: Structural variant discovery by integrated paired-end and split-read analysis. *Bioinformatics* **28**, i333–i339 (2012).
60. X. Chen *et al*., Manta: Rapid detection of structural variants and indels for germline and cancer sequencing applications. *Bioinformatics* **32**, 1220–1222 (2016).
61. J. A. Wala *et al*., SvABA: Genome-wide detection of structural variants and indels by local assembly. *Genome Res.* **28**, 581–591 (2018).

Downloaded at Palestinian Territory, occupied on November 27, 2021

www.manaraa.com